Optics and Lasers in Engineering 154 (2022) 107041

Contents lists available at ScienceDirect

Optics and Lasers in Engineering

journal homepage: www.elsevier.com/locate/optlaseng

# Positioning of diffuse metallic target with a point diffractive interferometer

Justo Arines[a,b,*], Alba Candal-Parafita[c], Jose Luís Martín-Iglesias[c]

[a] Departamento de Física aplicada, Facultad de Óptica y Optometría, Campus Vida, Universidad de Santiago de Compostela, 15782, Spain
[b] Instituto de Materiais (iMATUS), Campus Vida, Universidad de Santiago de Compostela, 15782, Spain
[c] Instituto de Educación Secundaria Arcebispo Xelmirez II, Rúa Irmandiños, 15, Santiago de Compostela 15704, Spain

A B S T R A C T

Proton acceleration obtained by focusing an ultraintense ultrafast laser beam presents the technological and metrological challenge of correctly placing diffuse metallic target at the focus of the laser beam. In this work we present the use of the Point diffractive interferometer for solving this problem. We studied the accuracy and precision of the system at repositioning the metallic target after displacing and horizontally tilting the target out of its reference position. We achieved an accuracy at repositioning the target at its reference position of 1.50 μm and 6 arcmin with a precision of 1.40 μm and 5.7 arcmin. Our work shows the high accuracy provided by a system as simple as the Point Diffraction interferometer even at positioning surfaces with diffuse reflection.

## 1. Introduction

Positron emission tomography is a non-invasive nuclear medicine technique that allows the metabolism of an organism to be studied. It is based on the administration of a radioactive isotope that is obtained from the collision of accelerated protons on a base substance. The most used method to bombard the target is based on the use of cyclotrons that accelerate the protons. An alternative method is to focus an ultrafast, ultra-intense laser on a metallic target [1–4]. In this system, it is essential to have a setup that allows the placement and orientation of the metallic target with respect to the beam focus to achieve the threshold irradiance and get the accelerated protons in the correct direction. As the target moves away from the focus plane, the irradiance of the laser beam diminishes limiting the amount and energy of the accelerated protons Fig. 1 presents the general scheme used in this kind of systems. An ultrafast ultraintense laser beam is directed onto an off-axis parabola (OAP) that focuses the beam at plane $\Pi_{in\text{-}focus}$. Let's call $\Pi_{target}$ the plane containing the metallic target and $\Pi_{out\text{-}focus}$ any plane out of focus. In the case that $\Pi_{in\text{-}focus} \neq \Pi_{target}$ the irradiance over the target would not be maximum, compromising proton extraction. Likewise, it is also important to orient the target correctly, considering that the ejection of accelerated protons is perpendicular to its surface. Beside, during light matter interaction at the surface of the target at the irradiances used in proton acceleration, material from the surface of the target is expelled at high velocities perpendicular to its surface, with the risk of damaging the optics found in their path.

Different systems have been proposed for the correct placement of the metallic target in this context. Researchers from the University of Valencia opted for Speckle interferometry, reaching an uncertainty in the relocation of the metallic target of 25 μm [1]. On the other hand, the group of McKenna et al. mounted a target repositioning system on the Rutherford Appleton laboratory Astra laser. Their system consisted of using a laser line parallel to the high-power laser focused on the metallic target. The retroreflected beam was collected by a system that imaged the metallic target in such a way that by seeing the degree of focus of the beam they could reposition the target. With their system they achieved a precision of 25 μm [2]. Beside, they pointed that with their setup, an error of 25 μm out of focus means a reduction of the intensity from $3.09 \times 10^{19}$ Wcm$^{-2}$ to $2.10 \times 10^{19}$ Wcm$^{-2}$ (a reduction of the 30%). Similarly, Ref. [3] presents a retroreflective system used to measure the stability of the position of a moving tape used as target. They found a wobbling of the tape around 14 μm. Likewise, Vallières et al. [4] combined a shadowgraphy system and a Michelson interferometer in the 200TW ALLs laser of the INRS-EMT of Varennes (Canada) with which they achieved a precision in the repositioning of the metal target of 20 μm and 1 μm respectively. Recently Shou et al. [5] proposed the use of microscale transparent dots placed on transparent targets as phase objects to develop a positioning system. Phase objects become visible out of focus and invisible in focus. Combining this property with a telescopic system they were able to achieve a precision of 2 μm in the positioning of their targets. A different setup was proposed by Burdonov et al. [6] achieving a precision of 20 μm. They developed a system using two beams focalized and overlapped at the focal plane of the OAP, so that when the reflective target was at the focal plane, the telescopic system used to guide the alignment showed one tiny spot. By contrast when the target was out of focus the system showed two tiny spots, whose separation depended on the position of the target.

The accuracy in the relocation of the metallic target is relevant in comparison with the depth of focus of the OAP. In this context it is important to define the depth of focus in relation to the reduction in the

* Corresponding author at: Departamento de Física aplicada, Facultad de Óptica y Optometría, Campus Vida, Universidad de Santiago de Compostela, 15782, Spain.
*E-mail address:* justo.arines@usc.es (J. Arines).

https://doi.org/10.1016/j.optlaseng.2022.107041
Received 26 November 2021; Received in revised form 8 March 2022; Accepted 9 March 2022
Available online 16 March 2022

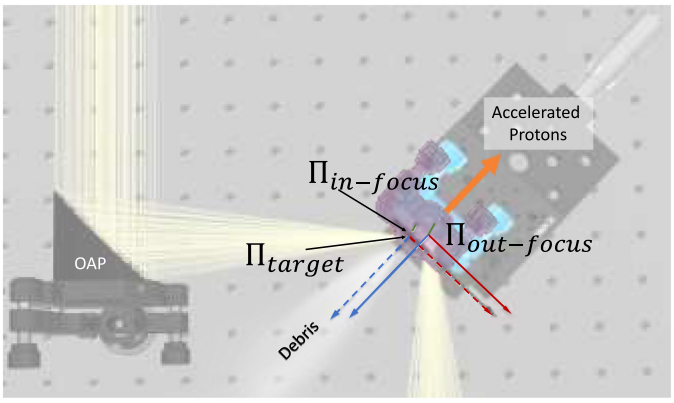


**Fig. 1.** Proton acceleration by laser focusing.

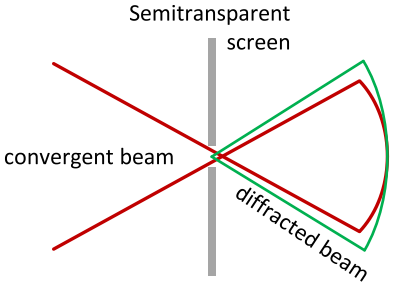


**Fig. 2.** PDI scheme.

peak of the irradiance distribution. Following the work of Urey [7] the depth of focus of a truncated gaussian beam of 3 cm of full width at 1/e, focused by a lens with 5 cm aperture and 15 cm focal length, is around 12 μm. Considering this value, the methods described in Refs. [1,2] do not provide enough accuracy if used with a laser beam and OAP as those used for the numerical example. The system described in Ref. [3], based in a Michelson interferometer provide enough accuracy but by increasing complexity and cost.

The works described above presents different setups for repositioning metallic and transparent targets that suffered an axial displacement, but none of them studied tip-tilt misorientation. Axial displacement affects irradiance distribution, but tip-tilt affects direction of proton extraction, which is also important.

In the present work we propose a simple system based on the point diffraction interferometer (PDI) [8], to reposition diffuse metallic targets that have undergone displacement and horizontal tilt of its surface with respect to the incident beam and direction of reference. The proposed system is simple and can be placed far from the laser plume and out of its direction of propagation, reducing the deterioration of its optics by debris generated during light matter interaction at the target surface.

## 2. Point diffraction interferometer

The point diffraction interferometer (PDI) is a remarkably simple common path interferometer [8–12]. This interferometer is based on focalizing a laser beam on a transparent hole placed on a semitransparent screen. Let's define $\Pi_{PH}$ the plane containing the screen. After crossing the screen, two waves emerge, one is the incident wave, while the second is the diffracted wave. These two waves propagate in the same direction and interfere giving rise to an interferogram. This simple description shows the simplicity of the PDI. The interference pattern depends on the impinging wavefront and the relative position of the hole with respect to the plane where the beam converges Fig. 2 shows the diagram of the PDI. The intensity distribution at the detection plane (Eq. (1)) is a combination of three terms; the first term corresponds to the diffracted beam; the second to the transmitted wave; and the third is the interferometric term [9,10].

**Table 1**
List of elements of the setup.

| Laser | Thorlabs HTPS-EC, $\lambda = 650$ nm |
|---|---|
| Spatial filter | |
| L1 | $f = 15$ cm; $D = 5$ cm |
| L2 | $f = 7.5$ cm; $D = 5$ cm |
| OAP | $f = 15$ cm; $D = 5$ cm |
| Translation stage | Resolution; 0.5 μm |
| Rotation stage | Resolution; 5 arcmin |
| Semitransparent pinhole | Diameter; 15 μm |
| Camera | Thorlabs USB 3.0 |
| Target | Aluminum foil; size, 4 × 2.5 cm$^2$; 500 μm thick |

$f$ = focal length; $D$ = diameter.

$$I(x_o, y_o) = a^4 J inc^2 \left(\frac{akr_o}{R}\right) + \left(\frac{Rt}{\frac{k}{\varepsilon}(R-\varepsilon)}\right)^2 + 2a^2 J inc \left(\frac{akr_o}{R}\right)\left(\frac{Rt}{\frac{k}{\varepsilon}(R-\varepsilon)}\right)\cos(\gamma) \quad (1)$$

where $\gamma = \frac{k}{2R}[\frac{\varepsilon}{(R-\varepsilon)}((x_o + X_{PH})^2 + (y_o + Y_{PH})^2)]$, $a$ is the diameter of the hole; $k$ is the wave number; $r_o$, $x_o$, $y_o$ are the radial and cartesian coordinates in the observation plane ($\Pi_D$); $X_{PH}$ and $Y_{PH}$ are the coordinates of the center of the transparent hole contained in plane $\Pi_{PH}$; $R$ is the distance between $\Pi_{PH}$ and $\Pi_D$; $t$ is the transmittance of the semitransparent sheet; and $\varepsilon$ is the separations between the plane where the beam converges ($\Pi'$) and $\Pi_{PH}$. So, when $\Pi' = \Pi_{PH}$, we get $\varepsilon = 0$ and second and third term of Eq. (1) are cancelled, being the intensity at the detection plane just due to diffraction. By contrast, if $\Pi' \neq \Pi_{PH}$, $\varepsilon \neq 0$ and what we observe at the detection plane is a combination of the three terms, that depends on the value of $\varepsilon$. So, as $\Pi'$ get closer to $\Pi_{PH}$ the number of fringes of the interferometric pattern diminishes progressively while the intensity of the diffraction pattern increases.

Consider now the configuration shown at Fig. 3. Lens L2 conjugates plane $\Pi_{in\text{-}focus}$ with $\Pi_{PH}$ and $\Pi_{out\text{-}focus}$ with $\Pi'$. If the reflective target is at $\Pi_{in\text{-}focus}$, then $\varepsilon = 0$ and $I(x_o, y_o) = a^4 J inc^2(\frac{akr_o}{R})$ (diffraction term). However, if the target is at $\Pi_{out\text{-}focus}$ then $\varepsilon \neq 0$ and the intensity distribution changes (involving all terms of Eq. (1)). Therefore, it would be possible to reposition the target ($\Pi_{target}$) to the reference position at $\Pi_{in\text{-}focus}$ just by observing and recovering the reference intensity distribution. This is the basis of the method that we propose in this work for repositioning diffuse reflecting metallic targets.

## 3. Experimental setup and methodology

The proposed positioning system has been shown in Fig. 3. The setup shows lens L2 at 45° from the normal of the metallic target, at a distance $S$ from $\Pi_{in\text{-}focus}$ to avoid the reception of the metallic debris expelled during the proton acceleration process. As said before, lens L2 conjugates plane $\Pi_{in\text{-}focus}$ (plane where the OAP focuses the laser beam, and reference position for the metallic target), with the plane containing the semitransparent screen of the PDI ($\Pi_{PH}$).

In Fig. 4 we show the experimental setup built to test our proposal, and in Table 1 the corresponding list of elements. The setup comprises a laser; a spatial filter; lens L1 to expand and collimate the beam to a diameter of 3 cm at 1/e; OAP to focalize the beam at plane $\Pi_{in\text{-}focus}$; a diffuse reflective metallic target; a holder placed on a rotating platform mounted above a translation stage, so that we can move axially and tilt horizontally the target. In the configuration of Fig. 4, $S = 22.7$ cm. The semitransparent screen of the PDI is placed at $\Pi_{PH}$ at 11.25 cm from L2 in a XY translation stage. Finally, we placed a digital camera at the detection plane ($\Pi_D$). The lower left corner of Fig. 4 shows the intensity

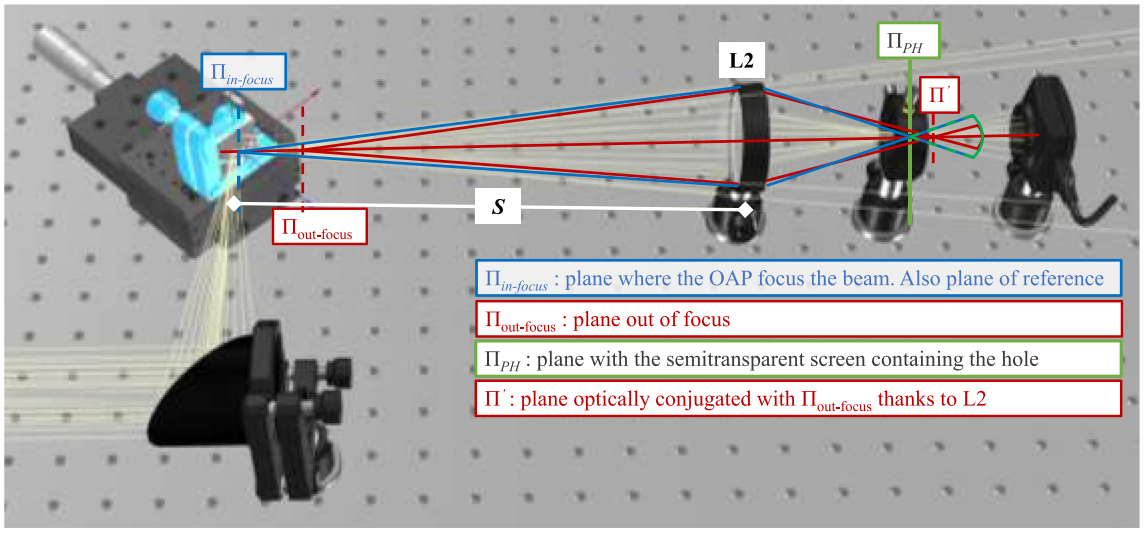


**Fig. 3.** Method basic scheme.

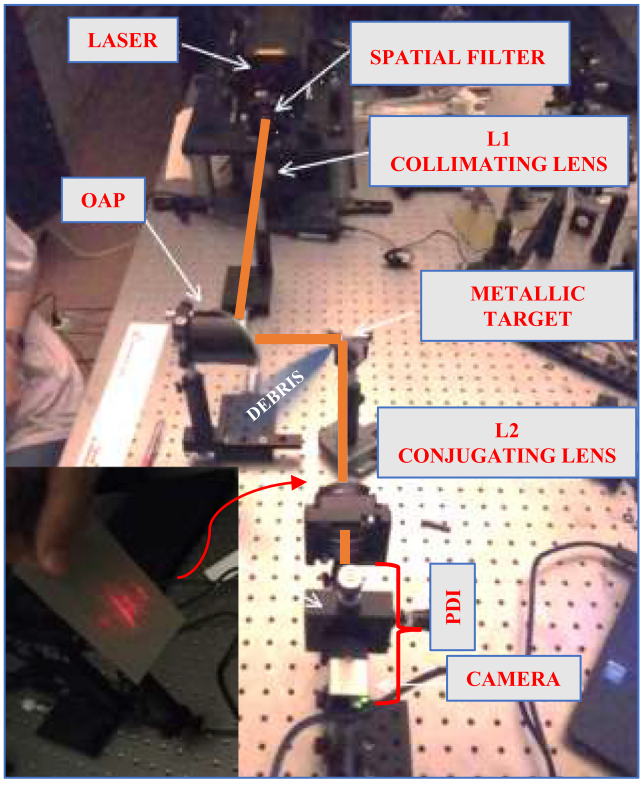


**Fig. 4.** Experimental setup.

distribution just before L2, after the reflection on the diffusive metallic target.

The positioning system was built following the next steps: 1) we placed the metallic target at the focus of the OAP; 2) we set $S = 22.7$ cm from $\Pi_{\text{in-focus}}$; 3) the semitransparent pinhole screen was placed at the conjugate plane of $\Pi_{\text{in-focus}}$. This position was found by observing the images provided by the camera up to the moment we obtained an intensity distribution resembling the diffraction pattern without interference fringes (as in Fig. 5, $\Delta x = 0$ μm). Once the PDI is adjusted it is no longer changed. In a second round of measurements, we increased $S$ to 48.5 cm. In consequence we adjusted the position of the semitransparent pinhole as described previously.

During the validation of the system, we used the following methodology: (1) a member of the team moves the metallic target away from its initial position; (2) a different member (who did not see how the movement was made) proceeded to reposition the target in its initial position with no help other than visualizing of the real time images provided by the camera. We repeated the procedure several times with different amounts of displacements. The same procedure was followed combining the axial displacement and horizontal tilt of the metallic target.

Fig. 5 shows the irradiance distribution at the detection plane for three different positions of the target ($\Delta x = \Pi_{\text{in-focus}} - \Pi_{\text{target}}$). In the case of $\Delta x = 500$ μm we can see the interferometric pattern at the left side of the figure. As we approach the target to $\Pi_{\text{in-focus}}$, the region with fringes moves to the center of the image and increase the size while the number of fringes diminishes. In the second image $\Delta x = 50$ μm we have an intermediate situation where no interferometric fringes can be seen. Finally, when $\Delta x = 0$ μm we get a significant increase in intensity dominated by the diffracted pattern.

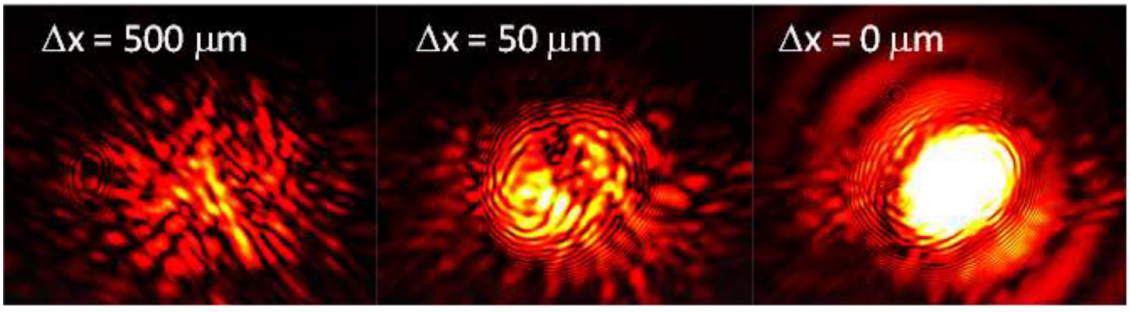


**Fig. 5.** Images at different positions of the target.

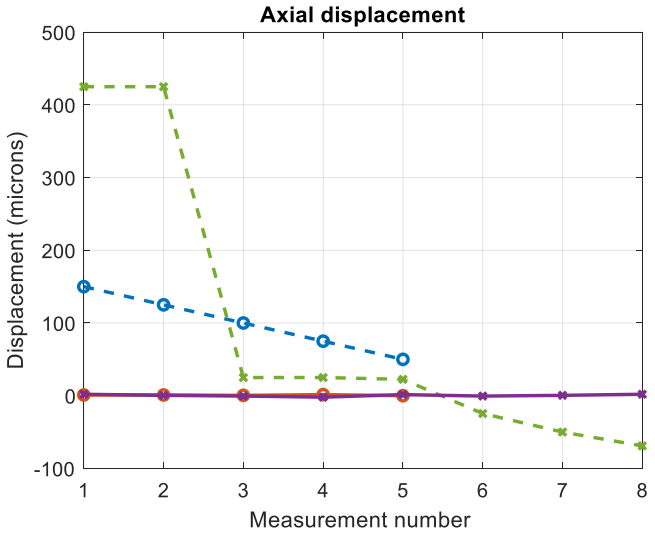


**Fig. 6.** Induced axial translation (dashed lines) and final position after repositioning the target (solid lines) for $S$ = 22.7 cm (green and purple lines); $S$ = 48.5 cm (red and blue lines).

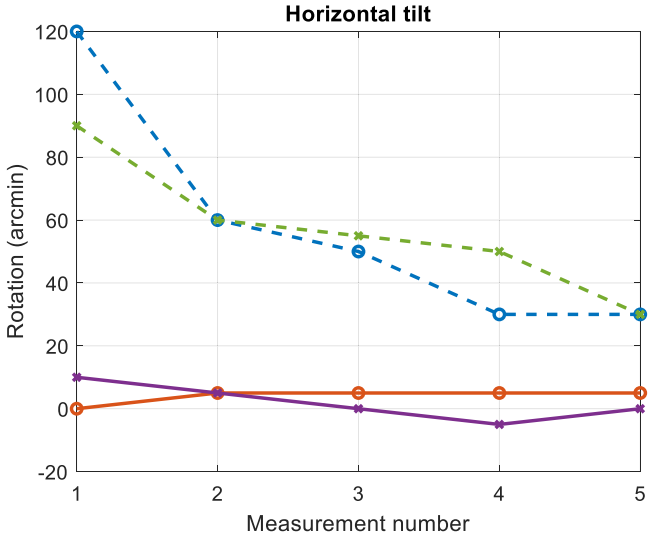


**Fig. 7.** Induced horizontal tilt (dashed lines) and final position after repositioning the target (solid lines) for $S$ = 22.7 cm (green and purple lines); $S$ = 48.5 cm (red and blue lines).

## 4. Results

We tested the system for two values of $S$ (22.7 cm and 48.5 cm). In both cases we evaluated the accuracy and precision at repositioning the target at its original position after suffering certain amount of axial translation, horizontal tilt, and combination of translation and horizontal tilt Figs. 6–8 show the results obtained during the measurements.

In Table 2 we show the accuracy and precision achieved with the proposed system for the two positions of L2. The results obtained in both cases are compatible although different. Considering the worst values, the accuracy provided by the system at repositioning the target after axial translation and/or horizontal tilt is 1.5 μm and 6.0 arcmin with a precision of 1.40 μm and 5.7 arcmin.

After finishing the measurements presented in Figs. 6 to 8, we removed the semitransparent pinhole and placed in its place the digital camera with the idea of comparing our proposal with the method of using the image of the focal spot at the target. In this way we mimic the

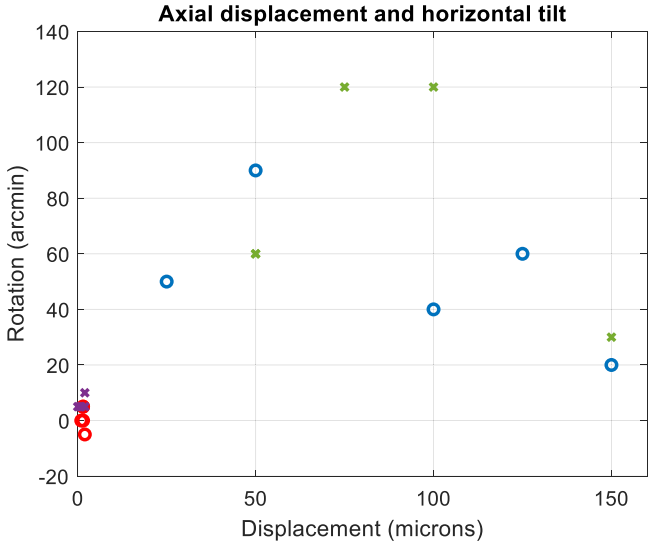


**Fig. 8.** Induced axial translation and horizontal tilt (dashed lines) and final position after repositioning the target (solid lines) for the $S$ = 22.7 cm (green and purple lines); $S$ = 48.5 cm (red and blue lines).

**Table 2**
Accuracy and precision.

| | $S$ = 22.7 cm | $S$ = 48.5 cm |
|---|---|---|
| Translation | accuracy: 0.44 μm<br>precision:1.40 μm | accuracy: 0.80 μm<br>precision: 0.57 μm |
| Rotation | accuracy: 2.0 arcmin<br>precision: 5.7 arcmin | accuracy: 4.0 arcmin<br>precision: 2.3 arcmin |
| Translation + Rotation | accuracy: 1.50 μm; 1.0 arcmin<br>precision: 0.35 μm; 4.2 arcmin | accuracy: 1.10 μm; 6.0 arcmin<br>precision: 0.89 μm; 2.3 arcmin |

retroreflective setup proposed in Ref. [2]. In Fig. 9 we show the images obtained for 5 different positions of the metallic target, separated 25 μm between each of them. Image 3 corresponds with the target at $\Pi_{in\text{-}focus}$. The shape of the spot is not regular due to the diffuse surface of the metallic target hampering the detection of the best position. Pictures 2, 3 and 4 are remarkably similar providing a range of ±25 μm in which it is very difficult to decide which is the best position.

PDI has a remarkable detection precision specially for those PDI with diffraction holes of the order of the wavelength. However, for such small holes the system is difficult to align presenting a limited dynamic range. The PDI used in this manuscript (with diameter of 15 μm) enters the category of Hole diffraction interferometer (HDI) developed by Prof. Acosta et al. [10]. This modification of the PDI uses a hole of size significantly bigger that the beam wavelength, providing high dynamic range and easy alignment, at the cost of reducing its sensitivity.

PDI systems are normally used to measure wavefront aberrations or 3D positions with high accuracy [11–13]. In both cases information is extracted from the recorded interferograms. These applications suffer from systematic errors and are susceptible to environmental changes. Different solutions have been developed to reduce these factors [14,15].

By contrast, in this work we use the PDI to reposition a diffuse metal target just by observing the image at the detection plane, without performing any operation on it. No wavefront calculation, no ring / line counting, just visual comparison between the reference image obtained at the reference position of the target, and the image obtained during the repositioning process. By proceeding in this way, we are overcoming the systematic error introduced by the non-ideal diffracted spherical wavefront or the wavefront extraction algorithm.

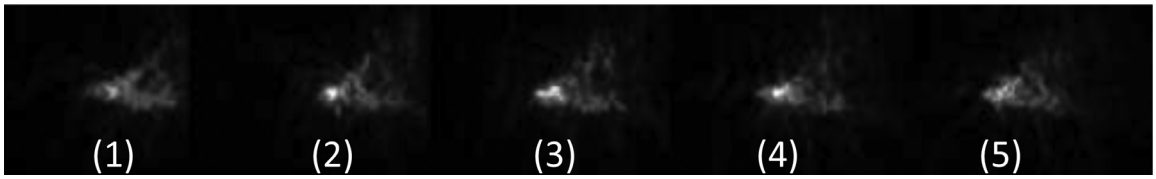


**Fig. 9.** Focal spot obtained at 5 positions of the metallic target spaced 25 μm between them.

Beside, the experiment presented in this work was carried out over an optical table with no antivibration system, placed on the corridor of an open laboratory with high air flow for good ventilation due to the Sars-CoV-2 pandemic, with people walking around the table. At each experimental session we started by defining the reference position. This procedure, in combination with the big size of the hole of the PDI, contribute to desensitize the system to environmental changes that can occur between experimental sessions. Considering the environmental conditions under which we conducted the experiments, the precision achieved is a good indicator of the robustness of the proposed method.

## 5. Conclusions

Tight focusing is crucial for many applications. In laser-driven proton acceleration being out of focus means a drastic reduction on proton extraction. Different methods have been proposed in the literature for positioning the target at the correct place: low or high magnification telescopes; shadowgraphy; Michelson interferometry; or the use of phase objects. In this work we presented a new method based on the use of a point diffractive interferometer for positioning non-mirrored metallic target such as those used in the proton acceleration. In this work we analyzed the accuracy and precision of the system at repositioning the target after suffering axial translation. Beside, we studied the performance after horizontal tilt of the target, study that most of the works related with this topic skipped. The proposed method is simple, precise, and reliable, allowing the repositioning of the target with an accuracy of 1.50 μm and 6 arcmin with a precision of 1.40 μm and 5.7 arcmin, overcoming the performance of other systems developed for the same purposes.

## Declaration of Competing Interest

The authors declare that they have no known competing financial interests or personal relationships that could have appeared to influence the work reported in this paper.

## CRediT authorship contribution statement

**Justo Arines:** Conceptualization, Methodology, Investigation, Formal analysis, Writing – original draft, Funding acquisition. **Alba Candal-Parafita:** Investigation, Formal analysis, Writing – original draft, Supervision. **Jose Luís Martín-Iglesias:** Methodology, Writing – original draft, Supervision.

## Acknowledgments

This work has been conducted within the framework of the STEM-BACH program (STEM-bach and Baccalaureate of excellence in science and technology) of the Consellería de Cultura, Educación e Ordenación Universitaria, Xunta de Galicia. This work has been founded by Consellería de Cultura, Educación e Ordenación Universitaria, Xunta de Galicia (ED43B 2020/29).

## References

[1] J. Pablo, B. Millán, Caracterización de protones acelerados por láser y estudio de aplicaciones médicas. Valencia, Doctoral thesis. https://dialnet.unirioja.es/servlet/tesis?codigo=180584, 2013.
[2] McKenna P, Ledingham KWD, Spencer I, McCany T, Singhal RP. Characterization of multiterawatt laser-solid interactions for proton acceleration. Rev Sci Instrum 2002;73(12):4176–84. doi:10.1063/1.1516855.
[3] Noaman-ul-haq M, et al. Statistical analysis of laser driven protons using a high-repetition-rate tape drive target system. Phys Rev Accel Beams 2017;20:041301. doi:10.1103/PhysRevAccelBeams.20.041301.
[4] Vallières S, Puyuelo-Valdes P, Salvadori M, et al. The laser-driven ion acceleration beamline on the ALLS 200 TW for testing nanowire targets. In: Proceedings of the laser acceleration of electrons, protons, and ions; 2019. V, 1103703.
[5] Shou Y, et al. Automated positioning of transparent targets using defocusing method in a laser proton accelerator. Nucl Instrum Methods Phys Res A 2019;927:236–9. doi:10.1016/j.nima.2019.02.034.
[6] Burdonov K, et al. Characterization and performance of the Apollon short-focal-area facility following its commissioning at 1 PW level. Matter Radiat Extremes 2021;6:064402. doi:10.1063/5.0065138.
[7] Urey H. Spot size, depth-of-focus, and diffraction ring intensity formulas for truncated Gaussian beams. Appl Opt 2004;43:620–5. doi:10.1364/AO.43.000620.
[8] Smartt RN, Steel WH. Theory and application of point-diffraction interferometers. Jpn J Appl Phys 1975;14:351.
[9] Chamadoira Hermida, S., Interferómetro de difracción por orificio, IDO, para la inspección y caracterización de lentes progresivas. Universidade de Santiago de Compostela, PhD Thesis, 2011. https://minerva.usc.es/xmlui/bitstream/handle/10347/4349/rep_181_2012.pdf?sequence=1&isAllowed=y
[10] Acosta E, Chamadoira S, Blendowske R. Modified point diffraction interferometer for inspection and evaluation of ophthalmic components. J Opt Soc Am A 2006;23:632–7. doi:10.1364/JOSAA.23.000632.
[11] Gargallo A, Arines J, Acosta E. Lens aberrations and their relationship with lens sutures for species with Y-suture branches. J Biomed Opt 2013;18(2):025003. doi:10.1117/1.JBO.18.2.025003.
[12] Bueno JM, Acosta E, Schwarz C, Artal P. Wavefront measurements of phase plates combining a point-diffraction interferometer and a Hartmann-Shack sensor. Appl Opt 2010;49(3):450–6. doi:10.1364/AO.49.000450.
[13] Rhee HG, Chu J, Lee YW. Absolute three-dimensional coordinate measurement by the two-point diffraction interferometry. Opt Express 2007;15(8):4435–44. doi:10.1364/OE.15.004435.
[14] Gao F, O'Donoghue T, Wang W. Full-field analysis of wavefront errors in point diffraction interferometer with misaligned Gaussian incidence. Appl Opt 2020;59(1):210–16. doi:10.1364/AO.59.000210.
[15] Sun Y, Shen H, Li X, Li J, Gao J, Zhu R. Wavelength-tuning point diffraction interferometer resisting inconsistent light intensity and environmental vibration: application to high-precision measurement of a large-aperture spherical surface. Appl Opt 2019;58(5):1253–60. doi:10.1364/AO.58.001253.